PCCP

PAPER

Cite this: *Phys. Chem. Chem. Phys.*, 2016, **18**, 6175

Superhalogen properties of BS_2^- and BSO^-: photoelectron spectroscopy and theoretical calculations

Li-Juan Zhao, Hong-Guang Xu, Gang Feng, Peng Wang, Xi-Ling Xu* and Wei-Jun Zheng*

Received 12th December 2015,
Accepted 20th January 2016

DOI: 10.1039/c5cp07673k

www.rsc.org/pccp

We investigate BS_2^- and BSO^- clusters using photoelectron spectroscopy and theoretical calculations. The electron affinities of BS_2 and BSO are measured to be 3.80 ± 0.03 and 3.88 ± 0.03 eV, respectively, higher than those of halogen atoms. Thus, BS_2 and BSO can be considered as superhalogens. The comparison of experimental and theoretical results confirmed that the ground state structures of BS_2^-, BSO^-, and their neutrals are all linear. Analyses of natural bond orbitals suggest that both BS_2^- and BSO^- have dual 3c-4e π hyperbonds.

1. Introduction

The term of superhalogen was first proposed by Gutsev and Boldyrev to classify a series of species with electron affinities (EAs) higher than those of halogen atoms.[1–3] Owing to their high electron affinities,[4–9] superhalogens are strong oxidizers that can interact with a wide variety of species to form new materials.[10–17] The varied structures and electronegativities of different superhalogens give us more ability to tune the properties of functional materials.[18–20] BO_2 has been studied extensively in the last decades.[21–37] It can be considered as a superhalogen because it is only one electron away from having a closed electronic shell and has a high electron affinity of 4.46 eV.[38] Recent studies show that BO_2 can be used as a building block for new superhalogens and hyperhalogens.[39–44] BS_2 and BSO are isoelectronic to BO_2. It has been suggested by theoretical calculations that BS_2 is a superhalogen similar to BO_2 and may act as a building block for hyperhalogens.[45,46] Utilization of BS_2 or its analogues can provide new opportunities for the design and synthesis of novel hyperhalogen species. The absorption spectra of BS_2 were measured in neon matrices[47] and in the gas phase.[48] The Renner–Teller effect, spin–orbit splitting, and K-resonance effects of BS_2 were investigated with laser-induced fluorescence techniques.[49–51] Until now, there has been no experimental measurements on the electron affinities of BS_2 and BSO in the literature. Studies on BSO are scarce. In this work, we conducted a combined photoelectron spectroscopy and theoretical study on BS_2^- and BSO^-. Our experimental measurements show that the electron affinities of both BS_2 and BSO surpass those of the halogens, thus, confirm that both BS_2 and BSO are superhalogens. The chemical bonding and electronic properties of BS_2^- and BSO^- are also analyzed.

Beijing National Laboratory for Molecular Sciences, State Key Laboratory of Molecular Reaction Dynamics, Institute of Chemistry, Chinese Academy of Sciences, Beijing 100190, China. E-mail: xlxu@iccas.ac.cn, zhengwj@iccas.ac.cn; Fax: +86 10 62563167; Tel: +86 10 62635054

2. Experimental and theoretical methods

2.1 Experimental method

The experiments were conducted on a home-built apparatus consisting of a laser vaporization cluster source, a time-of-flight (TOF) mass spectrometer, and a magnetic-bottle photoelectron spectrometer, which has been described elsewhere.[52] Briefly, the BS_2^- and BSO^- anions were produced by laser ablation of a rotating and translating boron–sulfur mixture disk target (13 mm diameter, B/S mole ratio 40 : 1) with the second harmonic of a nanosecond Nd:YAG laser (Continuum Surelite II-10). The typical laser power used in this work was about 10 mJ per pulse. Helium carrier gas with ~4 atm back pressure was used to cool the formed clusters by expanding through a pulsed valve (General Valve Series 9) into the source. $^{11}BS_2^-$ and $^{11}BSO^-$ clusters were each selected using a mass gate, decelerated by a momentum decelerator, and photodetached with the beam of another Nd:YAG laser (Continuum Surelite II-10; 266 nm) or an ArF excimer laser (PSX-100, 193 nm). The photoelectrons produced were energy-analyzed using the magnetic-bottle photoelectron spectrometer. The photoelectron spectra were calibrated using the spectra of Cu^- and Au^- obtained under similar conditions. The resolution of the photoelectron spectrometer was about 40 meV at the electron kinetic energy of 1 eV.

2.2 Theoretical method

The structures of BS_2^- and BSO^- as well as those of their corresponding neutral species were optimized using the Becke three-parameter hybrid exchange functional combined with the Lee–Yang–Parr correlation functional (B3LYP) method[53,54] with augmented correlation-consistent polarized valence triple-zeta basis sets (aug-cc-pVTZ)[55] which are obtained from the EMSL basis set exchange.[56] Optimizations of each species started from all possible structural candidates with full relaxation of each atom's position without any symmetry restrictions. The singlet and triplet multiplicities of BS_2^- and BSO^- as well as the doublet and quadruplet of their neutrals were all considered in the current work. Harmonic vibrational frequency analyses were implemented in order to make sure that the obtained structures were real local minima. The relative energies of all the optimized structures were then single-point calculated with the coupled cluster theory with single, double and non-iterative triple excitations (CCSD(T))[57–59] and the same basis sets as those used in the optimization step. The harmonic vibrational frequencies of BSO^- and its neutral counterpart were also calculated at the CCSD(T)/aug-cc-pVTZ level of theory. The relative energies were used to estimate the vertical detachment energies (VDEs) and the adiabatic detachment energies (ADEs) of BS_2^- and BSO^-, in which the VDE is defined as the energy difference between the neutral and anion both at the equilibrium structure of the anion, whereas the ADE is the energy difference between the neutral and the anion with the neutral relaxed to the nearest local minimum using the anionic structure as the initial structure. Molecular orbital (MO) analyses were conducted to investigate the bonding character. Wiberg bond indexes (WBI) and reference Lewis resonance structures of BS_2^- and BSO^- were obtained from the natural bond orbital (NBO) analyses.[60] All calculations were performed using the Gaussian 09 program package.[61]

3. Experimental results

The photoelectron spectra of $^{11}BS_2^-$ and $^{11}BSO^-$ obtained at 266 nm and 193 nm photon energies are shown in Fig. 1. The ADEs and VDEs of BS_2^- and BSO^- evaluated from the photoelectron spectra are summarized in Table 1 and are compared with the calculated ADEs and VDEs of different isomers at the CCSD(T)//B3LYP/aug-cc-pVTZ level of theory.

The 266 nm spectrum of the BS_2^- cluster has only a sharp peak centered at 3.80 eV, labeled X. In addition to the peak X, another band (A) centered at ~5.56 eV is also observed in the 193 nm spectrum. The top of band A extends from 5.52 eV to 5.61 eV probably due to the unresolved vibrational peaks. No vibrational progression of peak X is seen in the 266 and 193 nm

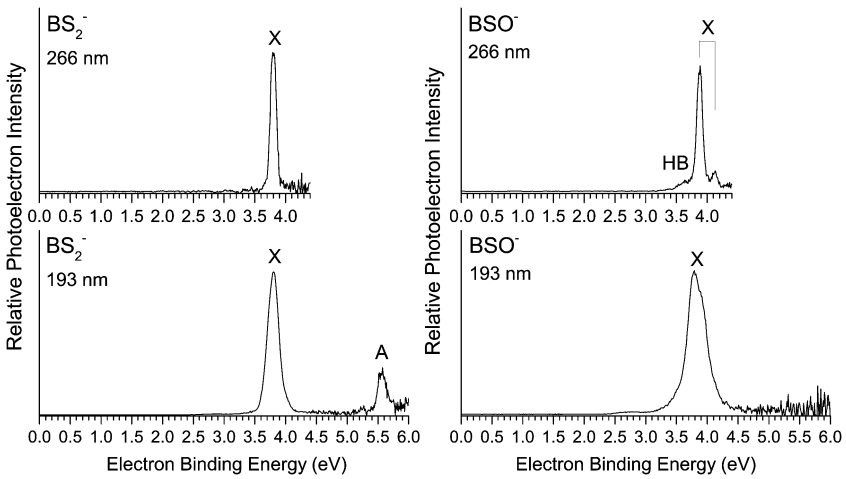

Fig. 1 Photoelectron spectra of BS_2^- and BSO^- recorded with 266 nm and 193 nm photons.

Table 1 Relative energies, ADEs and VDEs of the low-lying structures of BS_2^- and BSO^- calculated at the CCSD(T)//B3LYP/aug-cc-pVTZ level of theory along with the experimental ADEs and VDEs determined from the photoelectron spectra of BS_2^- and BSO^-

					ADE (eV)			VDE (eV)		
					Theo.			Theo.		
Isomer				ΔE (eV) CCSD(T)	B3LYP	CCSD(T)	Expt.	B3LYP	CCSD(T)	Expt.
BS_2^-	1A	$D_{\infty h}$	$^1\Sigma_g^+$	0.00	3.69	3.78	3.80(3)[a]	3.69	3.78	3.80(3)[a]
	1B	C_{2v}	$^3B_2$	3.33	0.52	0.45		1.79	1.64	
BSO^-	2A	$C_{\infty v}$	$^1\Sigma^+$	0.00	3.82	3.81	3.88(3)[a]	3.85	3.85	3.88(3)[a]
	2B	C_s	$^3A'$	3.81	0.15	−0.01		1.42	1.22	

[a] The numbers in parentheses indicate the uncertainties of the experimental values in the last digits.

spectra of BS_2^-, which means little geometry change between the ground states of BS_2^- and its neutral. Therefore, peak X defines both the ADE and VDE of BS_2^- as 3.80 eV. The ADE of BS_2^- equals the EA of its corresponding neutral, BS_2. As band A in the spectrum represents the transition from the ground state of BS_2^- anion to the first excited state of neutral BS_2, the term energy of the first electron excited state of neutral BS_2 is estimated to be 1.72 ± 0.03 eV based on the space between peak X and the front part of band A, which is in agreement with the value (1.716 eV) determined from the laser-induced fluorescence experiment.[51]

For BSO^-, only one relatively broad peak was observed at 193 nm. In the 266 nm spectrum, that broad peak is resolved into a major peak centered at 3.88 eV, a small peak at 4.13 eV, and a shoulder centered at 3.64 eV. The shoulder at 3.64 eV is a "hot band" resulting from the vibrational excited BSO^- anion. The spacing between the "hot band" and the major peak is about 0.24 eV (1936 cm^{-1}), consistent with the ^{11}B–O stretching frequency of BSO^- anion. The spacing between the small peak and the major peak is about 0.25 eV (2016 cm^{-1}), which is close to the ^{11}B–O stretching frequency of neutral BSO. More details will be shown in Section 4.

4. Theoretical results

As shown in Fig. 2, the most stable isomer of BS_2^- (1A) is a $D_{\infty h}$ linear structure in the $^1\Sigma_g^+$ electronic state. Its ADE/VDE values are calculated to be 3.78/3.78 eV at the CCSD(T) level of theory, in good agreement with experimental ADE/VDE values (3.80/3.80 eV). The second isomer of BS_2^- (1B) is a C_{2v} bent structure with a ∠SBS bond angle of 117°. It is in the $^3B_2$ electronic state and is higher in energy than 1A by 3.33 eV. Its ADE/VDE values are calculated to be 0.45/1.64 eV at the CCSD(T) level of theory, much lower than the experimental ones. That confirms that isomer 1A is the ground state structure of BS_2^- and is the one contributing to the photoelectron spectra of BS_2^-. The most stable isomer of neutral BS_2 (1a) is also a linear structure similar to the anionic structure (1A). It has $D_{\infty h}$ symmetry and is in the $^2\Pi_g$ electronic state. The second isomer of neutral BS_2 (1b) is higher in energy than isomer 1a by 2.01 eV. Our calculations indicate that the geometric change between the ground states of the BS_2^- anion (1A) and BS_2 neutral (1a) is very small. That can explain why no vibrational progression of peak X is observed in the 266 nm spectrum.

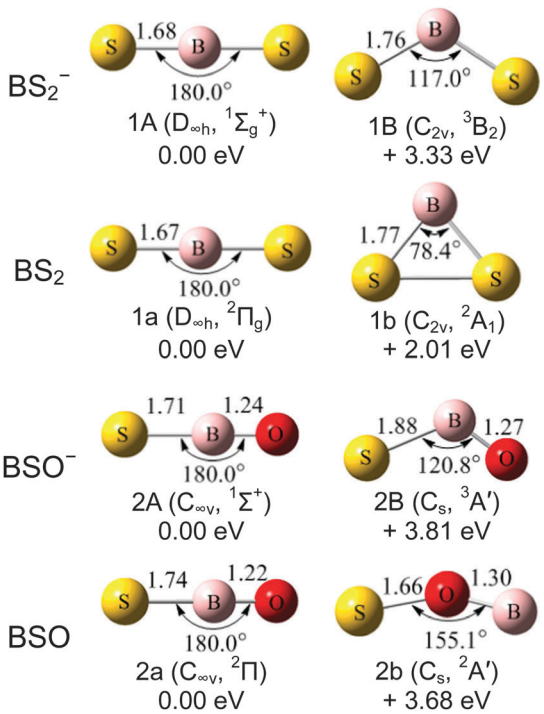

Fig. 2 Low-lying isomers of BS_2^-, BSO^-, and their neutrals. The bond lengths (in Å) and bond angles are also labeled. The relative energies to the most stable isomers are obtained using single-point calculations at the CCSD(T)/aug-cc-pVTZ level of theory.

The most stable isomer of BSO^- (isomer 2A) is a $C_{\infty v}$ linear structure in the $^1\Sigma^+$ electronic state (Fig. 2). The ADE/VDE values of isomer 2A are calculated to be 3.81/3.85 eV at the CCSD(T) level of theory, in agreement with the experimental ADE/VDE values of BSO^- (3.88/3.88 eV). The ^{11}B–O stretching frequency of S–^{11}B–O for the BSO^- anion is calculated to be 1804 cm^{-1} (0.22 eV) at the B3LYP level of theory and 1834 cm^{-1} (0.23 eV) at the CCSD(T) level of theory, consistent with the energy gap (0.24 eV) between the "hot band" and the major band X in the 266 nm spectrum of BSO^-. Isomer 2B is a C_s bent structure in the $^3A'$ electronic state with a ∠SBO bond angle of 121° and its calculated ADE/VDE values are −0.01/1.22 eV at the CCSD(T) level of theory, much lower than the experimental ones. Furthermore, isomer 2B is higher in energy than 2A by 3.81 eV. Thus, it is unlikely for isomer 2B to be present in the experiment. Isomer 2A is the most probable structure of BSO^- observed in the experiment. Similar to the BSO^- anion, the most stable structure of neutral BSO (2a) is a $C_{\infty v}$ linear structure in the $^2\Pi$ electronic state. The ^{11}B–O stretching frequency of neutral BSO is calculated to be 1825 cm^{-1} (0.23 eV) at the B3LYP level of theory and 1904 cm^{-1} (0.24 eV) at the CCSD(T) level of theory, in good agreement with the vibrational progression (0.25 eV) observed in the 266 nm spectrum of BSO^-. Note here the calculated frequencies of BSO^- and BSO are lower than the experimental values instead of being higher than the experimental values, indicating that the general frequency scale factor for the B3LYP method[62] cannot be applied here.

5. Discussion

5.1 Molecular orbital analyses

According to the theoretical results in Table 1, the ground state structures of both the BS_2^- and BSO^- anions are linear structures with closed-shell electronic states. Their corresponding valence molecular orbitals are shown in Fig. 3. The valence electronic configuration of BS_2^- is $(1\sigma_g)^2(1\sigma_u)^2(2\sigma_g)^2(2\sigma_u)^2(1\pi_u)^4(1\pi_g)^4$. The two HOMOs of BS_2^- are degenerate π_g orbitals, nearly all from $3p_x$ (or $3p_y$) lone pairs of the S atom and the percentage of each S atom is 50%. The geometric parameters between BS_2^-

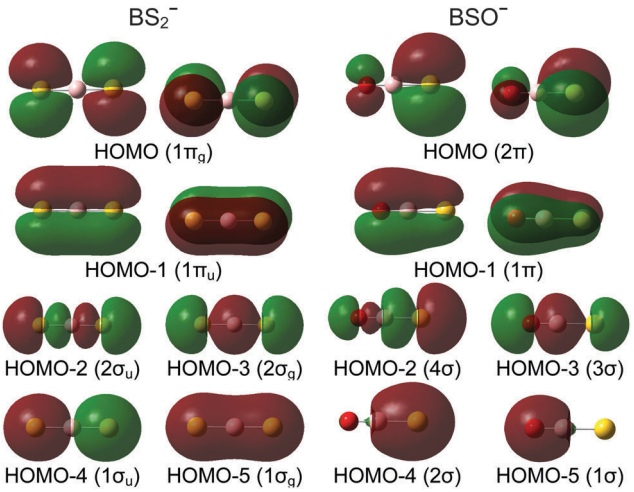

Fig. 3 The diagrams of the valence molecular orbitals of the ground state structures of the BS_2^- and BSO^- anions.

and their corresponding neutrals are nearly the same, consistent with the non-bonding electronic character of the HOMO orbitals. The HOMO−1s are also degenerate orbitals, which correspond to strong S–B–S π bonds. They consist mostly of the outmost shell p_x or p_y of the S atoms and B atom. The HOMO−1 in the p_x (or p_y) manifold has 34% S1, 34% S2, and 31% B3. One electron detaching from these π bonds will produce the first electronic excited state ($^2\Pi_u$) of BS_2, and weaken the bond significantly. The HOMO−2 ($2\sigma_u$) orbital is primarily composed of the $3p_z$ of the S atoms (38% for each) and the $2p_z$ of the B atom (11%). The HOMO−3 ($2\sigma_g$) mainly comprises the $3p_z$ of S and 2s of B. For HOMO−4, the 3s of S and $2p_z$ of B constitute $1\sigma_u$. The HOMO−5 ($1\sigma_g$) is a strong σ bond, mainly from the outmost s components of the B and S atoms.

The valence electronic configuration of BSO^- is $(1\sigma)^2(2\sigma)^2(3\sigma)^2(4\sigma)^2(1\pi)^4(2\pi)^4$. For BSO^-, the $2p_x$ of O (15%), $3p_x$ of S (82%), and $2p_x$ of B (3%) compose one 2π HOMO orbital, and their outmost p_y orbitals compose another degenerate HOMO orbital. Similar to the HOMOs of BS_2^-, the HOMOs of BSO^- are also non-bonding orbitals. Its degenerate HOMO−1s correspond to the strong S–B–O π bonds, which consist mostly of the outmost shell p_x or p_y of the S atom, O atom, and B atom. The HOMO−1 in the p_x or p_y manifold consists of the p_x or p_y atomic orbitals of B (23%), S (7%), and O (70%) atoms. When detaching one electron from these π bonds, the first electronic excited state ($^2\Pi$) of BSO forms. $2p_z$ of O (14%), $3p_z$ of S (59%), 3s of S (11%), 2s of B (7%) and $2p_z$ of B (8%) participate in composing the HOMO−2 (4σ). The HOMO−3 (3σ) mainly comprises the $3p_z$ of S, 2s of B and $2p_z$ of O. Only the S (3s) and B (2s, $2p_z$) atoms form the 2σ. Similarly, almost all the electron clouds of HOMO−5 (1σ) locate on O (80%) and B (18%), consisting of their s and p_z atomic orbitals.

5.2 Reference resonance Lewis structures of BS_2^- and BSO^-

Based on the NBO analyses, the schematic resonance Lewis structures of the ground state of BS_2^- and BSO^- are shown in Fig. 4. For BS_2^-, three resonance structures are found. Among them, the former two NRTs (NRT1 and NRT2) have one S–B single bond and one S≡B triple bond. The weightings of them are nearly the same (∼34%), more than that of NRT3 with two S=B double bonds (∼30%). Moreover, four pairs of lone electrons are found in each of NRT1, NRT2 and NRT3. The Wiberg bond index (WBI) of B–S in BS_2^- is calculated to be 1.784. Unlike BS_2^-, BSO^- has only two resonance structures. NRT1 has one S–B single bond and one B≡O triple bond, the weighting of which is ∼10% more than that of NRT2 with two double bonds. In addition, each of NRT1 and NRT2 has four pairs of lone electrons. For BSO^-, the WBI of B–S is 1.541 and that of B–O is 1.491. Thus, it can be seen that the double-bond character of the B–S bond is stronger in BS_2^- than in BSO^-.

5.3 Charge analyses

Natural population analyses at the CCSD(T) level were used to investigate the charge distributions of the ground state structures of BS_2^- and BSO^- and the natural charge of each atom is presented in Table 2. In BS_2^-, the charges on the S1 and S2 atoms are both −0.645 *e*, and that on the B3 atom is +0.290 *e*. This indicates negative charge mainly locates on the S atoms, which is consistent with the electronegative sequence of the free B and S atoms. For BSO^-, the natural charges on the B1, S2, and O3 atoms are +0.893 *e*, −0.827 *e*, and −1.066 *e*, respectively. In comparison with BS_2^-, the charges distributing in BSO^- tell us that the negative charge is mainly located on the O3 atom, and the S2 atom gets more negative charge compared to that in BS_2^- and the B1 atom loses an extra ∼0.6 electrons under the existence of a more electronegative O atom.

Moreover, the low occupancy (1.73 *e*) of the S1 lone pairs and high occupancy (0.26 *e*) of π^*_{B3S2} and the large estimated n_{S1}–π^*_{B3S2} second-order perturbation energy (99.73 kcal mol^{-1}) for BS_2^- are consistent with the strong resonance delocalization and charge transfer in BS_2^-. Likewise, strong resonance delocalization and charge transfer also exist in BSO^-, which are confirmed by the low occupancy (1.82 *e*) of the S2 lone pairs and

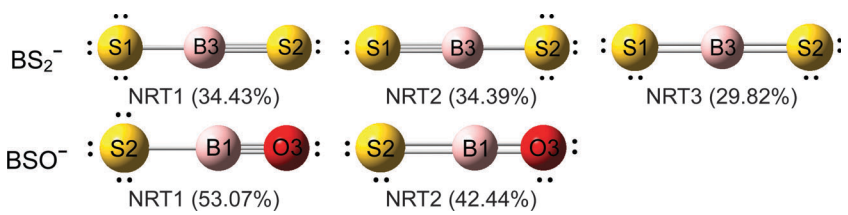

Fig. 4 Schematic reference resonance Lewis presentations for the ground state structures of BS_2^- and BSO^-. Single bonds, triple bonds and lone-pairs are labeled. The numbers in the parentheses are the weightings of each NRT structure at the CCSD(T) level of theory.

Table 2 NPA charge distributions in the most stable isomers of the BS_2^- and BSO^- anions at the CCSD(T) level of theory

Cluster	Atom	NPA charge (e)	Cluster	Atom	NPA charge (e)
BS_2^-	S1	−0.645	BSO^-	B1	0.893
	S2	−0.645		S2	−0.827
	B3	0.290		O3	−1.066

high occupancy (0.17 *e*) of π^*_{B1O3} and the large estimated n_{S2}–π^*_{B1O3} second-order perturbation energy (64.63 kcal mol^{-1}) for BSO^-.

5.4 Dual 3c-4e π hyperbonds

According to the NBO analyses, dual 3-center 4-electron hyperbonds (3c-4e π-bonds) are found in both BS_2^- and BSO^-, which has already been explored in binary, ternary and quaternary boron oxide systems, such as $B_4O_4^-$, $LiB_2O_3^{-/0}$, $AuB_2O_3^{-/0}$, and $LiAuB_2O_3^{-/0}$ clusters.[63,64] Such 3c-4e hyperbonds from the localized NBO perspective are more aptly described in Coulson's picture[65] as a strong resonance hybrid of two localized Lewis structure representations, S1:B3–S2 ↔ S1–B3:S2 for BS_2^- and S2:B1–O3 ↔ S2–B1:O3 for BSO^-, which can be denoted with the special symbols S1:–B3–:S2 and S2:–B1–:O3 for each. For BS_2^-, the two degenerate HOMOs are virtually non-bonding and the two degenerate HOMO−1s are π bonds. Thus, the HOMOs and HOMO−1s form dual 3c-4e π hyperbonds in the p_x and p_y manifolds. Likewise, the degenerate HOMOs and HOMO−1s of BSO^- also constitute its dual 3c-4e π hyperbonds. Such 3c-4e π hyperbonds of BS_2^- or BSO^- are similar to the 3c-4e σ hyperbond (ω-bond) in FHF^-,[66] except that the former are π bonds, whereas the latter in fact are σ bonds.

The large estimated n_{S1}–π^*_{B3S2} and n_{S2}–π^*_{B1O3} second-order perturbation energies and charge transfers are all consistent with strong S1:–B3:–S2 and S2:–B1:–O3 hyperbond character, respectively. To some extent, the 3c-4e hyperbonds account for the delocalized bonding in BS_2^- and BSO^-, which also explain their HOMO−1 π orbitals in some perspective.

5.5 Comparison to BO_2

The photoelectron spectra of BS_2^- and BSO^- are similar to those of BO_2^-.[38] The adiabatic electron affinities of BS_2, BSO, and BO_2 are 3.80, 3.88, and 4.46 eV, respectively, all larger than those of the halogens, indicating that they are all superhalogens. Obviously, the electron affinity of BO_2 is the largest while that of BS_2 is the smallest. That is to say, for these three neutrals, the number of oxygen atoms has a great influence on their electron affinities. Their electron affinities decrease with a decreasing number of O atoms. It is interesting that the first substitution of an O atom by an S atom reduces the electron affinity significantly by 0.58 eV while the second substitution of an O atom by an S atom lowers the electron affinity by only 0.08 eV. As it has been mentioned in the molecular orbital analyses section, the HOMOs of BS_2^- and BSO^- (SOMOs of BSO and BS_2) are mainly contributed by the p orbitals of the S atoms, while that of BO_2^- (SOMO of BO_2) is mainly contributed by the p orbitals of the O atoms. The SOMOs of both BSO and BS_2 are mainly affected by the p orbitals of the S atom and the energies of the p orbitals of the S atom are much higher than the energies of the p orbitals of the O atom. That may explain why the electron affinities of BS_2 and BSO are close to each other and much lower than that of BO_2. It has been reported that BO_2 can be used as a building block for hyperhalogens such as $Au(BO_2)_2$, $Cu(BO_2)_2$, $Na(BO_2)_2$ and $Al(BO_2)_2$.[67] Whether BS_2 and BSO can be used as building blocks for new hyperhalogens remains to be investigated by theoretical and experimental studies. In fact, BS_2 has been suggested as a building block for hyperhalogens such as $Au(BS_2)_2$ by theoretical calculations.[46] However, there is no report of related aspects of BSO. More efforts are needed to further explore the applications of BS_2 and BSO.

6. Conclusions

In summary, we have studied the structural, electronic and bonding character of BS_2^- and BSO^- anions using photoelectron spectroscopy and theoretical calculations. The electron affinities of BS_2 and BSO are estimated to be 3.80 ± 0.03 and 3.88 ± 0.03 eV, respectively. The fact that the electron affinities of BS_2 and BSO are larger than those of halogens confirms their superhalogen identities. The ground state structures of BS_2^- and BSO^- and their neutrals are all linear. Chemical bonding analyses show that both BS_2^- and BSO^- have dual 3c-4e π hyperbonds.

Acknowledgements

This work was supported by the Natural Science Foundation of China (Grant No. 21303214 to X. L. X. and 21273246 to W. J. Z.). The theoretical calculations were conducted on the ScGrid and DeepComp 7000 of the Supercomputing center, Computer Network Information Center of the Chinese Academy of Sciences.

References

1 G. L. Gutsev and A. I. Boldyrev, *Chem. Phys.*, 1981, **56**, 277–283.
2 G. L. Gutsev and A. I. Boldyrev, *Chem. Phys. Lett.*, 1984, **108**, 255–258.
3 G. L. Gutsev and A. I. Boldyrev, *Russ. Chem. Rev.*, 1987, **56**, 519.
4 X.-B. Wang, C.-F. Ding, L.-S. Wang, A. I. Boldyrev and J. Simons, *J. Chem. Phys.*, 1999, **110**, 4763–4771.
5 G. L. Gutsev, B. K. Rao, P. Jena, X.-B. Wang and L.-S. Wang, *Chem. Phys. Lett.*, 1999, **312**, 598–605.
6 X.-B. Wang, L.-S. Wang, R. Brown, P. Schwerdtfeger, D. Schröder and H. Schwarz, *J. Chem. Phys.*, 2001, **114**, 7388–7395.
7 X. Yang, X.-B. Wang, L.-S. Wang, S. Niu and T. Ichiye, *J. Chem. Phys.*, 2003, **119**, 8311–8320.
8 B. M. Elliott, E. Koyle, A. I. Boldyrev, X.-B. Wang and L.-S. Wang, *J. Phys. Chem. A*, 2005, **109**, 11560–11567.
9 J. Yang, X.-B. Wang, X.-P. Xing and L.-S. Wang, *J. Chem. Phys.*, 2008, **128**, 201102.

10 O. Graudejus, S. H. Elder, G. M. Lucier, C. Shen and N. Bartlett, *Inorg. Chem.*, 1999, **38**, 2503–2509.
11 M. Sobczyk, A. Sawicka and P. Skurski, *Eur. J. Inorg. Chem.*, 2003, 3790–3797.
12 A. N. Alexandrova, A. I. Boldyrev, Y.-J. Fu, X. Yang, X.-B. Wang and L.-S. Wang, *J. Chem. Phys.*, 2004, **121**, 5709–5719.
13 I. Anusiewicz, *Aust. J. Chem.*, 2008, **61**, 712–717.
14 K. Pradhan, G. L. Gutsev and P. Jena, *J. Chem. Phys.*, 2010, **133**, 144301.
15 P. Koirala, M. Willis, B. Kiran, A. K. Kandalam and P. Jena, *J. Phys. Chem. C*, 2010, **114**, 16018–16024.
16 K. Pradhan and P. Jena, *J. Chem. Phys.*, 2011, **135**, 144305.
17 K. Pradhan, G. L. Gutsev, C. A. Weatherford and P. Jena, *J. Chem. Phys.*, 2011, **134**, 234311.
18 S. A. Claridge, A. W. Castleman, S. N. Khanna, C. B. Murray, A. Sen and P. S. Weiss, *ACS Nano*, 2009, **3**, 244–255.
19 A. W. Castleman and S. N. Khanna, *J. Phys. Chem. C*, 2009, **113**, 2664–2675.
20 P. Jena, *J. Phys. Chem. Lett.*, 2015, **6**, 1119–1125.
21 A. Sommer, D. White, M. J. Linevsky and D. E. Mann, *J. Chem. Phys.*, 1963, **38**, 87–98.
22 D. E. Jensen, *J. Chem. Phys.*, 1970, **52**, 3305–3306.
23 T. R. Burkholder and L. Andrews, *J. Chem. Phys.*, 1991, **95**, 8697–8709.
24 V. G. Zakrzewski and A. I. Boldyrev, *J. Chem. Phys.*, 1990, **93**, 657–660.
25 J. R. Chow, R. A. Beaudet, W. Schulz, K. Weyer and H. Walther, *Chem. Phys.*, 1990, **140**, 307–316.
26 A. G. Maki, J. B. Burkholder, A. Sinha and C. J. Howard, *J. Mol. Spectrosc.*, 1988, **130**, 238–248.
27 K. Kawaguchi and E. Hirota, *J. Mol. Spectrosc.*, 1986, **116**, 450–457.
28 P. Császár, W. Kosmus and Y. N. Panchenko, *Chem. Phys. Lett.*, 1986, **129**, 282–286.
29 V. Saraswathy, J. J. Diamond and G. A. Segal, *J. Phys. Chem.*, 1983, **87**, 718–719.
30 K. G. Weyer, R. A. Beaudet, R. Straubinger and H. Walther, *Chem. Phys.*, 1980, **47**, 171–178.
31 M. A. A. Clyne and M. C. Heaven, *Chem. Phys.*, 1980, **51**, 299–309.
32 R. S. Lowe, H. Gerhardt, W. Dillenschneider, R. F. Curl and F. K. Tittel, *J. Chem. Phys.*, 1979, **70**, 42–49.
33 A. Fried and C. W. Mathews, *Chem. Phys. Lett.*, 1977, **52**, 363–367.
34 R. N. Dixon, D. Field and M. Noble, *Chem. Phys. Lett.*, 1977, **50**, 1–5.
35 D. K. Russell, M. Kroll, D. A. Dows and R. A. Beaudet, *Chem. Phys. Lett.*, 1973, **20**, 153–155.
36 J. V. Ortiz, *J. Chem. Phys.*, 1993, **99**, 6727–6731.
37 J. Agreiter, M. Lorenz, A. M. Smith and V. E. Bondybey, *Chem. Phys.*, 1997, **224**, 301–313.
38 H.-J. Zhai, L.-M. Wang, S.-D. Li and L.-S. Wang, *J. Phys. Chem. A*, 2007, **111**, 1030–1035.
39 M. Götz, M. Willis, A. K. Kandalam, G. F. Ganteför and P. Jena, *ChemPhysChem*, 2010, **11**, 853–858.
40 M. Willis, M. Götz, A. K. Kandalam, G. F. Ganteför and P. Jena, *Angew. Chem., Int. Ed.*, 2010, **49**, 8966–8970.
41 Y. Feng, H.-G. Xu, W. Zheng, H. Zhao, A. K. Kandalam and P. Jena, *J. Chem. Phys.*, 2011, **134**, 094309.
42 Y. Feng, G.-L. Hou, H.-G. Xu, Z.-G. Zhang and W.-J. Zheng, *Chem. Phys. Lett.*, 2012, **545**, 21–25.
43 H. Chen, X.-Y. Kong, W. Zheng, J. Yao, A. K. Kandalam and P. Jena, *ChemPhysChem*, 2013, **14**, 3303–3308.
44 X.-Y. Kong, H.-G. Xu, P. Koirala, W.-J. Zheng, A. K. Kandalam and P. Jena, *Phys. Chem. Chem. Phys.*, 2014, **16**, 26067–26074.
45 J. V. Ortiz, *Chem. Phys. Lett.*, 1993, **214**, 467–472.
46 L.-P. Ding, X.-Y. Kuang, P. Shao, M.-M. Zhong and Y.-R. Zhao, *RSC Adv.*, 2013, **3**, 15449–15456.
47 J. M. Brom Jr and W. Weltner Jr, *J. Mol. Spectrosc.*, 1973, **45**, 82–98.
48 A. G. Briggs and R. E. Simmons, *Spectrosc. Lett.*, 1986, **19**, 953–961.
49 S.-G. He, C. J. Evans and D. J. Clouthier, *J. Chem. Phys.*, 2003, **119**, 2047–2056.
50 S.-G. He and D. J. Clouthier, *J. Chem. Phys.*, 2004, **120**, 4258–4262.
51 S.-G. He, D. J. Clouthier, A. G. Adam and D. W. Tokaryk, *J. Chem. Phys.*, 2005, **122**, 194314.
52 H.-G. Xu, Z.-G. Zhang, Y. Feng, J. Yuan, Y. Zhao and W. Zheng, *Chem. Phys. Lett.*, 2010, **487**, 204–208.
53 A. D. Becke, *J. Chem. Phys.*, 1993, **98**, 5648–5652.
54 C. Lee, W. Yang and R. G. Parr, *Phys. Rev. B: Condens. Matter Mater. Phys.*, 1988, **37**, 785–789.
55 R. A. Kendall, T. H. Dunning and R. J. Harrison, *J. Chem. Phys.*, 1992, **96**, 6796–6806.
56 N. B. da Costa, R. O. Freire, A. M. Simas and G. B. Rocha, *J. Phys. Chem. A*, 2007, **111**, 5015–5018.
57 G. E. Scuseria and H. F. Schaefer, *J. Chem. Phys.*, 1989, **90**, 3700–3703.
58 J. Čížek, *Adv. Chem. Phys.*, John Wiley & Sons, Inc., 2007, pp. 35–89.
59 F. Holka, M. Urban, P. Neogrády and J. Paldus, *J. Chem. Phys.*, 2014, **141**, 214303.
60 E. D. Glendening, J. K. Badenhoop, A. E. Reed, J. E. Carpenter, J. A. Bohmann, C. M. Morales and F. Weinhold, *NBO 5.0*, Theoretical Chemistry Institute, University of Wisconsin, Madison, 2001.
61 M. J. Frisch, G. W. Trucks, H. B. Schlegel, G. E. Scuseria, M. A. Robb, J. R. Cheeseman, G. Scalmani, V. Barone, B. Mennucci, G. A. Petersson, H. Nakatsuji, M. Caricato, X. Li, H. P. Hratchian, A. F. Izmaylov, J. Bloino, G. Zheng, J. L. Sonnenberg, M. Hada, M. Ehara, K. Toyota, R. Fukuda, J. Hasegawa, M. Ishida, T. Nakajima, Y. Honda, O. Kitao, H. Nakai, T. Vreven, J. A. Montgomery Jr., J. E. Peralta, F. Ogliaro, M. J. Bearpark, J. Heyd, E. N. Brothers, K. N. Kudin, V. N. Staroverov, R. Kobayashi, J. Normand, K. Raghavachari, A. P. Rendell, J. C. Burant, S. S. Iyengar, J. Tomasi, M. Cossi, N. Rega, N. J. Millam, M. Klene, J. E. Knox, J. B. Cross, V. Bakken, C. Adamo, J. Jaramillo, R. Gomperts, R. E. Stratmann, O. Yazyev, A. J. Austin, R. Cammi, C. Pomelli, J. W. Ochterski, R. L. Martin, K. Morokuma, V. G. Zakrzewski, G. A. Voth, P. Salvador,

J. J. Dannenberg, S. Dapprich, A. D. Daniels, Ö. Farkas, J. B. Foresman, J. V. Ortiz, J. Cioslowski and D. J. Fox, *Gaussian 09, revision D.01*, Gaussian, Inc., Wallingford, CT, USA, 2009.

62 Database of Frequency Scale Factors for Electronic Model Chemistries, http://comp.chem.umn.edu/freqscale/version3b2.htm.

63 W.-J. Tian, L.-J. Zhao, Q. Chen, T. Ou, H.-G. Xu, W.-J. Zheng, H.-J. Zhai and S.-D. Li, *J. Chem. Phys.*, 2015, **142**, 134305.

64 W.-J. Tian, H.-G. Xu, X.-Y. Kong, Q. Chen, W.-J. Zheng, H.-J. Zhai and S.-D. Li, *Phys. Chem. Chem. Phys.*, 2014, **16**, 5129–5136.

65 C. A. Coulson, *J. Chem. Soc.*, 1964, 1442–1454.

66 F. Weinhold and C. R. Landis, *Valency and Bonding: A Natural Bond Orbital Donor–Acceptor Perspective*, Cambridge University Press, Cambridge, 2005.

67 G. L. Gutsev, C. A. Weatherford, L. E. Johnson and P. Jena, *J. Comput. Chem.*, 2012, **33**, 416–424.